Journal of the Optical Society of America B
OPTICAL PHYSICS

Semiclassical calculation of the power saturation of the Kerr effect in Rb vapor

Zachary H. Levine[1,*] and Ziran Du[1,2]

[1]Quantum Measurement Division, National Institute of Standards and Technology, Gaithersburg, Maryland 20899, USA
[2]Department of Applied Mathematics and Statistics, State University of New York, Stony Brook, New York 11794, USA
*zlevine@nist.gov

Received 22 August 2023; revised 29 September 2023; accepted 17 October 2023; posted 30 October 2023; published 16 November 2023

The Kerr effect in atomic vapor may be regarded as the power saturation of the susceptibility. Hence the saturable Kerr effect is intimately tied to the standard Kerr effect. Here, we calculate the saturable Kerr effect without free parameters using a two-level system and find good agreement with experimental results. Our approach permits a direct comparison of theory to experiment without an extrapolation to low power as required by previous approaches. An experimentally observed asymmetry between red and blue detuning led us to consider a model with one ground state and three excited states. Such an asymmetry cannot be described by a two-state model. The model predicts about 25% of the observed asymmetry.

https://doi.org/10.1364/JOSAB.503903

1. INTRODUCTION

A theme of recent work in quantum optics is the manipulation of light at extremely low power levels, including the single-photon level. Among the many candidate media, rubidium vapor cells have been a subject of intensive study. Such cells are capable of generating quantum-correlated twin-beams [1,2] in addition to having several other applications including optical quantum memory [3], the characterization of thin layers using optical frequency combs [4], atomic clocks [5], sensitive magnetometers with application in biomedicine [6] and geology [7], gravimetry [8], and information encoding via cross-phase modulation [9]. Recent work includes the development of small, scalable vapor cells [10]. The field of optics with hot atomic vapors including rubidium has been reviewed recently [11].

All of these processes depend on nonlinear optics. Arguably the simplest nonlinear process is the Kerr effect, whereby the index of refraction in a medium is depending on the intensity of the light passing through it. In the Kerr effect, only one frequency and one polarization are required. Usually, the Kerr effect is regarded as a $\chi^{(3)}$ process, i.e., the induced polarization depends on the cube of the incident electric field. However, the thinking in nonlinear optics is heavily influenced by solid-state systems where the lowest-order perturbation theory is generally applicable for most practical systems. Atomic vapors exhibit nonlinear effects at very low power levels, which can be counterintuitive [12]. The saturation of the Kerr effect cannot be described through lowest-order perturbation theory. Yet, the Kerr effect for atomic vapor systems is routinely described in terms of the lowest-order perturbation theory [12–14], although these same papers describe experiments whose intensities are sufficient to induce O(1) changes in the magnitudes of the Kerr coefficient compared to its low-field (i.e., non-saturated) value. Recently, a second term in the perturbation expansion has been measured along with the Kerr coefficient in a cesium vapor cell [15].

Here, we calculate the Kerr coefficient at the electric fields for which it was measured, without extrapolating to the low-field regime. In addition to the question of principle, in practice, the Kerr coefficient varies rapidly at low power [12,14], making such extrapolation a source of uncertainty. Even now, there is some question about the precise value of the Kerr coefficient in rubidium vapor. For example, Araújo *et al.* report a 30% uncertainty for the extrapolated (i.e., non-saturated) Kerr coefficient in cesium [13], and a recent paper shows that the use of Gaussian–Bessel beams changes the value of the Kerr coefficient by a factor of 1.73 compared to a similar measurement with Gaussian beams [16].

Before our presentation of the theory, we note that there have been related studies of rubidium vapor cells. For example, the nonlinear absorption was measured on resonance 20 years ago [17], and the saturation of the Kerr effect has recently been extended to spatial mapping [18].

2. THEORY

We consider laser light incident on a Rb vapor cell. The light is treated as a monochromatic plane wave. The cell is assumed to have a uniform density of Rb atoms. We will consider only light with frequencies near the $5S_{1/2} \rightarrow 5P_{3/2}$ transition, known as the D2 line [19,20]. We consider continuous wave (CW) [12]

and pulsed [14] experiments. Both experiments use vapor cells that are short compared to the Rayleigh length of their Gaussian beams, and both measure the intensity in the center of the beam. In this case, we may calculate using a plane wave instead of a Gaussian.

We work in a semiclassical approximation, using the rotating wave approximation (RWA) [21,22] in quantum mechanics as well as the paraxial approximation in electrodynamics [23]. For the case of a two-level system, the susceptibility χ is given by [24]

$$\chi = -N\frac{d^2}{\epsilon_0\hbar}\frac{\Delta + i\frac{\Gamma_{sp}}{2}}{\frac{\Gamma_{sp}^2}{4} + \frac{\Omega_1^2}{2} + \Delta^2}, \tag{1}$$

where N is the number density, d is the dipole matrix element, ϵ_0 is the permittivity of free space, $\hbar$ is the reduced Planck constant, Γ_{sp} is the spontaneous emission rate, Ω_1 is the Rabi frequency at zero detuning, and Δ is the detuning. {See Eq. (2.188) in the reference. Angular frequencies must be used in Eq. (1) for Ω_1 and Δ; nevertheless we call these quantities "frequencies" and convert using 1 Hz $= 2\pi$ s^{-1} [25].} The expression assumes decoherence is due to spontaneous emission. We use the values $d = 2.52 \cdot 10^{-29}$ Cm [12,20] and $\Gamma_{sp} = 38.11 \cdot 10^6$ s^{-1}. The values change negligibly between ^{87}Rb and ^{85}Rb, so we use the same values for simplicity. The zero-detuning Rabi frequency is given by [24]

$$\Omega_1 = \frac{dE}{\hbar}, \tag{2}$$

where E is the amplitude of a real cosine wave electric field. Another key equation relates the electric field to the intensity in a plane wave. The formula is [26]

$$I = \frac{\epsilon_0 c n}{2}|\mathbf{E}|^2, \tag{3}$$

where c is the speed of light, and n is the index of refraction in the medium. In this work, we approximate $n = 1$ when using Eq. (3). The experiments [12,14] use a Gaussian beam, and they quote their results in terms of power. The power in a Gaussian beam is related to its peak intensity I_0 by

$$P = 2\pi\int_0^\infty \mathrm{d}\rho\, \rho I(\rho) = \frac{\pi w_0^2}{2} I_0 = \frac{z_R\lambda}{2} I_0, \tag{4}$$

where ρ is the radius used in cylindrical coordinates, w_0 is the beam waist parameter, z_R is the Rayleigh length, and λ is the wavelength. For the Rb D2 line, $\lambda = 780$ nm. Also, $z_R = 8$ mm is quoted in both experiments. Since the Rayleigh length is quoted in the references, we use the final form in Eq. (4) to convert intensity to power.

Both McCormick *et al.* [12] and Wang *et al.* [14] give a formula for the unsaturated Kerr effect for a two-level system. The formula may be derived from Eq. (1) and the other equations presented here by a first-order Taylor expansion in I [24] [Eq. (7B.9)]. Hence, the Kerr effect is the lowest-power manifestation of the saturation of the susceptibility; moreover, the two-level system predicts that the Kerr effect will also saturate. (Because $n^2 = 1 + \chi$, and $\chi \ll 1$ for the systems we consider, $n - 1 \approx \frac{1}{2}\chi$, so it does not matter qualitatively whether we consider the index or the susceptibility.) Representative values of conditions at saturation are given in Appendix A.

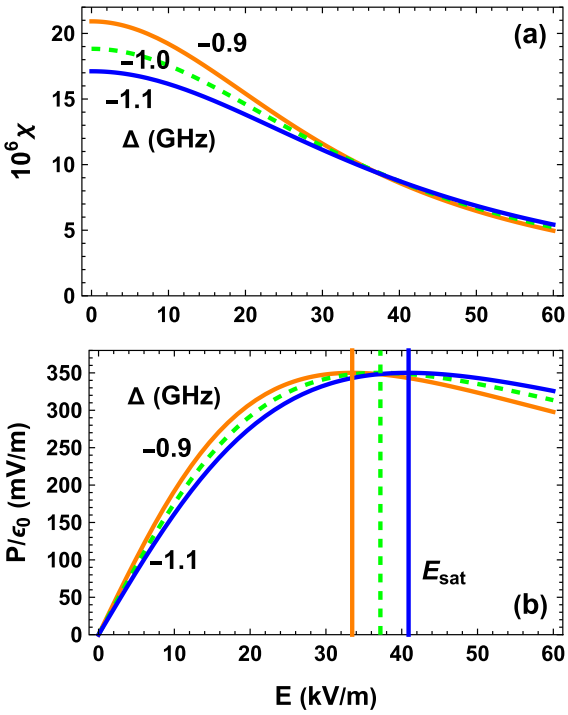

Fig. 1. Calculations for a two-level system red-detuned from the ^{87}Rb D2 line with a number density of $0.2783 \cdot 10^{18}$ m^{-3}. The dipole matrix element is taken to be $2.52 \cdot 10^{-29}$ Cm [12]. An occupancy factor of 5/8 is included to account for the fraction of atoms in the $F = 2$ state of the $5S_{1/2}$ state; (a) susceptibility and (b) polarization $P/\epsilon_0 = \chi E$. In (b), the saturation electric fields are shown, starting from $\Delta = -0.9$ GHz on the left. The orange, dashed green, and blue curves correspond to a detuning of $\Delta = -0.9$ GHz, -1.0 GHz, and -1.1 GHz, respectively. The electric fields corresponding to $s = 1$ are also shown.

The susceptibility of ^{87}Rb for the conditions of the experiment reported by McCormick *et al.* [12] is given in Fig. 1(a). Whereas McCormick *et al.* quote a number density of 10^{18} m^{-3}, the value used in our calculation is $0.2783 \cdot 10^{18}$ m^{-3} to account for the natural abundance of ^{87}Rb [20]. In addition, atoms in the $F = 1$ ground state are nearly noninteracting. As these represent 3/8 of the total, the number density is adjusted downward by an additional factor of 5/8, which is the fractional occupancy of the $F = 2$ ground state. The saturation effect leads the index of refraction to change its order as a function of Δ for sufficiently large electric fields. The susceptibility goes to zero as the field increases. Moreover, it does so quickly enough that the induced polarization peaks in absolute terms and also goes to zero as the incident electric field grows large, as shown in Fig. 1(b). Also shown are the saturation electric fields E_{sat}, which occur at the maxima of $P/\epsilon_0 = \chi E$.

The behavior may be understood qualitatively by considering Eqs. (A1)–(A3). For small electric fields, the saturation parameter is also small. If the detuning Δ is large compared to the spontaneous emission rate Γ_{sp}, then the susceptibility varies inversely with Δ, which explains the ordering at $E = 0$. As the electric field increases, the saturation parameter becomes large and contributes a factor of Δ^2 asymptotically. The product of

the two terms goes as Δ. Hence, the susceptibilities must appear in the opposite order as the electric field increases compared to the low-field limit.

The curvature at the beginning of the graph is related to the unsaturated Kerr effect. In general, we may find the saturated Kerr coefficient $n_2^{(s)}$ by

$$n_2^{(s)} = \frac{n(I) - n_0}{I}, \tag{5}$$

where $n(I)$ is the intensity-dependent index of refraction, and n_0 is its limit as $I \to 0$.

Some of our results include a calculation beyond the two-level system. For ^{87}Rb, we compute the density matrix within the RWA for a system consisting of the $F = 2$ ground-state level and the three excited-state levels with dipole allowed coupling, namely, $F' = 1, 2, 3$. As discussed in the text of Grynberg *et al.* [24], the susceptibility may be found through the steady state solution of the density matrix. In practice, we find this matrix by propagating the density matrix in time [27] by 0.5 μs, which is large compared to the lifetime of 28 ns and comparable to the typical time an atom spends in the beam. The formalism is given in Appendix B. The atom is initially taken to be in the ground state. The final time is a typical time that a Rb atom can spend in the beam. We considered the possibility of optical pumping to the $F = 1$ level. However, we found that this process occurs long after 0.5 μs for the detunings we consider. Near resonance, e.g., for $|\Delta| \le 10$ MHz, optical pumping would need to be included. Evaluating the density matrix in its steady state yields the induced dipole moment per atom p via

$$p = q_e \mathrm{Tr}(r\rho), \tag{6}$$

where q_e is the charge on the electron, r is the dipole operator, ρ is the density matrix computed within the RWA, and Tr is the trace. The polarization is given by $\mathcal{P} = Np$, where $\mathcal{P}$ is the polarization envelope, and N is the number density of atoms. This forms the source term in the paraxial wave equation, derived from the Maxwell equations. The equation is

$$\mathcal{E}_z + \frac{n_{\mathrm{bkg}}}{c}\mathcal{E}_t = \mathrm{i}\frac{\mu_0 c}{2n_{\mathrm{bkg}}}\omega\mathcal{P}, \tag{7}$$

where $\mathcal{E}$ is the electric field envelope, the subscripts z and t are the partial derivatives in the propagation direction and time, respectively, μ_0 is the vacuum permeability, n_{bkg} is the index of refraction due to effects that are not being modeled by the density matrix (i.e., the background), and ω is the optical frequency, about 384 THz. In practice, we take $n_{\mathrm{bkg}} = 1$. In the regime we consider, Clausius–Mossotti local field effects [26] may be neglected.

Strictly speaking, we should consider all of the magnetic sublevels when forming our density matrix. Coupling by spontaneous emission leads to the inclusion of many states. Nevertheless, non-magnetic systems are nearly always treated without considering magnetic sublevels. We do so here, but then we are faced with the question of determining the coupling coefficients. We find these by taking the coupling constants given by the Clebsch–Gordan-like formulas presented by Steck [19,20], squaring them, and summing them over the magnetic sublevels of a given transition. The values are given in Table 1.

Table 1. Matrix Elements Are the Positive Square Roots of the Following Quantities, which Are Sums of Squares of the Clebsch–Gordan-Like Coupling Constants Given by Steck [19,20][a]

^{85}Rb	$\|P_{3/2}F=1\rangle$	$\|P_{3/2}F=2\rangle$	$\|P_{3/2}F=3\rangle$	$\|P_{3/2}F=4\rangle$
$\|S_{1/2}F=2\rangle$	27/216	35/216	28/216	0
$\|S_{1/2}F=3\rangle$	0	10/216	35/216	81/216
^{87}Rb	$\|P_{3/2}F=0\rangle$	$\|P_{3/2}F=1\rangle$	$\|P_{3/2}F=2\rangle$	$\|P_{3/2}F=3\rangle$
$\|S_{1/2}F=1\rangle$	2/32	5/32	5/32	0
$\|S_{1/2}F=2\rangle$	0	1/32	5/32	14/32

[a]The entries in each pair of lines sum to one.

The matrix elements are the taken to be the positive square roots of these quantities. Using the positive signs is an assumption.

3. COMPARISON TO EXPERIMENT

In Fig. 2, the measured results for the saturated Kerr coefficient $n_2^{(s)}$ are given for the experiment of McCormick *et al.* [12] as well as the results of the two-level calculation. Extra lines are drawn in Fig. 2 that show that $s = 1$ is either in the middle of the range of the data or at the low end, depending on the case. In either case, only a non-perturbative calculation can be applied directly to make a comparison of the theory with the data at the power levels at which they were acquired.

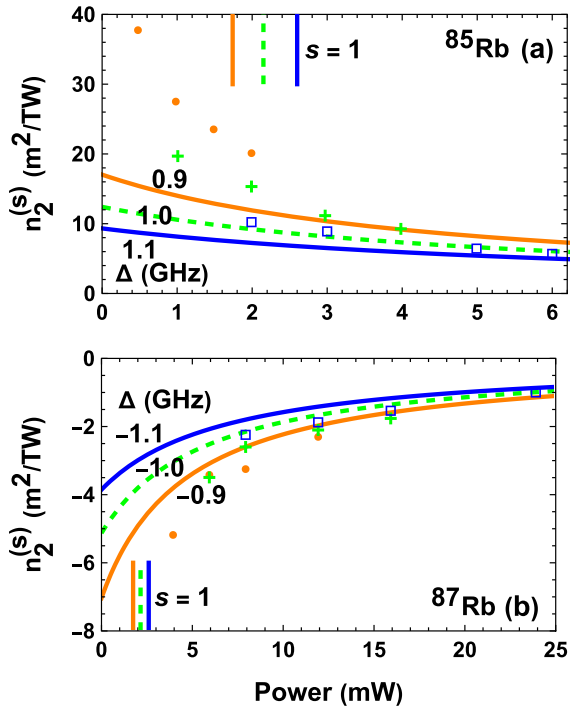

Fig. 2. Saturable Kerr coefficient $n_2^{(s)}$ as a function of CW power based on the experimental conditions of McCormick *et al.* [12] for (a) blue detuned ^{85}Rb and (b) red detuned ^{87}Rb. The filled orange circles, green plus symbols, and empty blue squares are taken from the reference with detuning of Δ of ± 0.9 GHz, ± 1.0 GHz, and ± 1.1 GHz, respectively. The same color assignments are used for the theoretical curves, including a dashed curve at ± 1.0 GHz. The three vertical lines in (a) and (b) correspond to the power for which $s = 1$ for (left to right) $|\Delta| = 0.9$ GHz, 1.0 GHz, and 1.1 GHz.

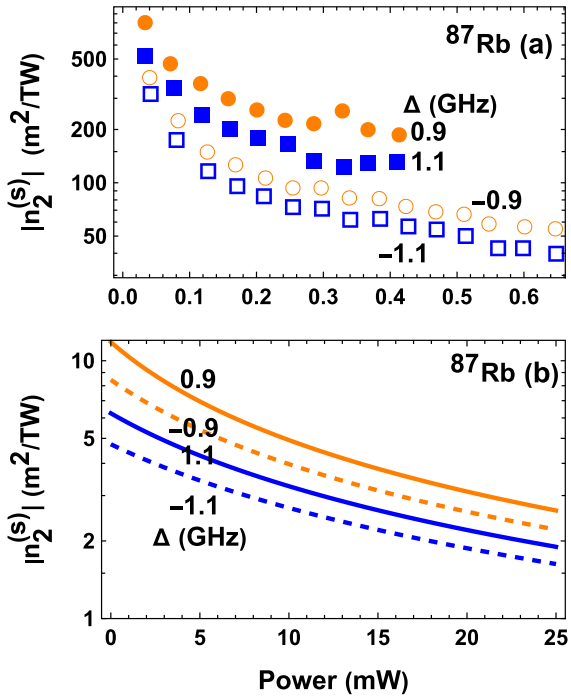

Fig. 3. Absolute value of $n_2^{(s)}$ (a) measured in isotopically pure ^{87}Rb with a pulsed laser and (b) computed including the ground state $F = 2$ level and the excited state $F = 1, 2, 3$ levels. The orange solid, orange dashed, blue solid, and blue dashed curves correspond to detunings $\Delta = 0.9$ GHz, -0.9 GHz, 1.1 GHz, and -1.1 GHz, respectively. The points are similar.

There are no adjustable parameters in the calculation, i.e., all values are tabulated or specified by the experiment. We find good quantitative agreement, with the calculated values being about 80% of the measured ones. The agreement of our model with the data is less good in the case of ^{85}Rb, although still within a factor of two. The experimental values vary more at low power than we can account for in the model. The two-level model is symmetric in the sign of Δ. Some of the difference between Figs. 2(a) and 2(b) is accounted for by the natural abundance ratio and the level degeneracy factors, leading to an expected greater value for ^{85}Rb of $(0.7217/0.2783)(7/12)/(5/8) = 2.4$, which is reflected in the theoretical curves. The cause of the remaining correction is obscure, although McCormick *et al.* [12] discuss the possibility of effects of the other isotope.

Wang *et al.* [14] used isotopically pure ^{87}Rb in their measurement. Selected values are given in Fig. 3(a). There is an asymmetry of about a factor of two, with blue detuning giving larger values than red detuning. The experiment of Wang *et al.* used a pulsed laser, so the results are not directly comparable to the theory or to the experiment of McCormick *et al.* As noted by Wang *et al.*, the reported values for the saturable Kerr coefficient are much larger than those obtained with static measurements. Part of this is due to having a higher density of Rb atoms (1.55× McCormick *et al.*) and part is due to using isotopically pure ^{87}Rb, which gives an enhancement factor of (1/0.2783), for a number-density-based enhancement of 5.6. This still leaves a large enhancement in the induced dipole moment per atom due to the pulses versus earlier CW measurements and the CW-based theory.

One source of this asymmetry is the fact that the transition moments grow with F' as shown in Table 1. The results of our calculation with one ground state and three excited states is shown in Fig. 3(b). We find an asymmetry factor of about 1.25, which is less than that factor of two implicit in the data of Wang *et al.* and also suggested by the McCormick *et al.* data.

4. CONCLUDING REMARKS

The saturable Kerr effect is a phenomenon closely related to the saturation of the susceptibility. The Kerr effect itself is a manifestation of the saturation of the susceptibility. Due to the low power levels required to achieve saturation, this is a practical consideration for contemporary experiments in rubidium vapor cells. The common assumption that a $\chi^{(5)}$ or $\chi^{(7)}$ phenomenon has to be smaller than a $\chi^{(3)}$ effect [14] does not apply if the saturation parameter $s \approx 1$.

We have achieved semiquantitative agreement with the experimental results for the intensity-saturation of the Kerr coefficient in rubidium vapor using a model of the two-level system with no adjustable parameters. (There are some parameters taken from other experiments, such as the dipole matrix element and the lifetime of the state.) There is an observed asymmetry in the response in the sign of detuning. We attempt to account for this asymmetry by considering three excited states instead of one, still in a framework with no adjustable parameters. Only about a quarter of this asymmetry can be accounted for by considering three excited states instead of one. Within the quantum mechanical domain, other effects to consider include Doppler broadening, relaxation effects, and light polarization [28], as well as a theory taking into account the pulsed beam. Obtaining full quantitative agreement may also depend on a more careful analysis of the transverse dependence of the electromagnetic interactions, given the sensitivity of the susceptibility to the incident power. Although the Kerr effect is the simplest nonlinear effect in rubidium vapor cells, open questions remain to achieve full quantitative understanding.

APPENDIX A: NUMERICAL ESTIMATE OF SATURATION POWER AND RELATED QUANTITIES

The linear susceptibility $\chi^{(1)}$ is the $\Omega_1 \to 0$ limit of Eq. (1), namely,

$$\chi^{(1)} = -N\frac{d^2}{\epsilon_0\hbar}\frac{\Delta + \mathrm{i}\frac{\Gamma_{\mathrm{sp}}}{2}}{\frac{\Gamma_{\mathrm{sp}}^2}{4} + \Delta^2}. \tag{A1}$$

Following Grynberg *et al.* [24], we may define the saturation parameter

$$s = \frac{\Omega_1^2/2}{\Delta^2 + \Gamma_{\mathrm{sp}}^2/4}. \tag{A2}$$

Equations (1), (A1), and (A2) imply

$$\chi = \chi^{(1)}\frac{1}{1+s}. \tag{A3}$$

Table 2. Parameters for the Rb D2 Line at Saturation ($s = 1$)[a]

Δ (GHz)	Ω_1 (GHz)	E (kV/m)	I (MW/m^2)	P (mW)
0	0.00303	0.113	$1.69 \cdot 10^{-5}$	$1.98 \cdot 10^{-5}$
1	1.41	37.2	184	2.15

[a]The values apply to both ^{85}Rb and ^{87}Rb to the accuracy quoted. The parameters $d = 2.52 \cdot 10^{-29}$ Cm, $\Gamma_{sp} = 38.11 \cdot 10^6$ s^{-1}, $n = 1$, $\lambda = 780$ nm, and $z_R = 8$ mm are used. The on-resonance Rabi frequency Ω_1, the electric field E, and the optical intensity I refer to the center of the Gaussian beam. The power P is integrated over a cross section of the beam at its waist.

The case of $s = 1$ is interesting since it occurs at the peak induced electric field, shown in Fig. 1(b). Since $s \propto E^2$, $s = 1$ also represents the value for which the perturbation series obeys $|\chi^{(1)}| = |\chi^{(3)}| = |\chi^{(5)}|$, etc., indicating a perturbative treatment is not warranted. Representative values on and off resonance are given in Table 2. Off resonance, $\Delta \propto \Omega_1 \propto E$ and $I \propto P \propto E^2$.

APPENDIX B: DENSITY MATRIX CALCULATION

The polarization $\mathcal{P}(t)$ is given by the RWA density matrix $\sigma(t)$ from

$$\mathcal{P}(t) = n_{\text{den}} q_e \text{Tr}\left(\mathbf{r}\sigma(t)\right). \tag{B1}$$

In the RWA, the time-dependent quantities vary slowly on the time-scale of an optical period (typically 3 fs) and are envelope functions. In practice, we use a 0.2 ns time step in our calculation, so there is about five orders of magnitude separation between the optical frequencies, which are treated analytically, and the slow radio-frequency variations, which are calculated.

The density matrix is governed by the Lindblad master equation

$$\frac{\mathrm{d}\sigma}{\mathrm{d}t} = -\mathrm{i}[H, \sigma] + \left.\frac{\mathrm{d}\sigma}{\mathrm{d}t}\right|_{\text{relax}} = \mathcal{L}\sigma, \tag{B2}$$

where H is the Hamiltonian, and $\frac{\mathrm{d}\rho}{\mathrm{d}t}|_{\text{relax}}$ describes the relaxation. Also, $\mathcal{L}$ is the Lindblad matrix, $\mathcal{L} = \mathcal{L}^{(L)} + \mathcal{L}^{(R)}$, with L for Liouville and R for relaxation. We model the relaxation as being due to spontaneous emission, which is a practical lower bound (i.e., in the absence of Purcell confinement effects). Without a buffer gas, collisions do not add significantly to decoherence rates. The elements of $\mathcal{L}^{(L)}$ are given as

$$\mathcal{L}^{(L)}_{ij,k\ell} = -\mathrm{i}H_{ik}\delta_{j\ell} + \mathrm{i}H_{\ell j}\delta_{ik}, \tag{B3}$$

where the indices i, j, k, ℓ run over the set of atomic basis states, H is the Hamiltonian matrix, and δ is the Kronecker δ. This equation is equivalent to Eq. (5) of Ref. [29]. The relaxation term $\mathcal{L}^{(R)}$ has nonzero elements for

$$\mathcal{L}^{(R)}_{kk,kk} = -\Gamma,\ \mathcal{L}^{(R)}_{ii,kk} = O_{ik}\Gamma,\ \mathcal{L}^{(R)}_{k\ell,k\ell} = -\frac{1}{2}\Gamma, \tag{B4}$$

where i is in the ground state manifold, and k and ℓ are in the excited state manifold. In Eq. (B4), Γ is the decay rate, and O is a matrix of branching ratios. The final line gives the decay of coherences under the assumption that these are due to spontaneous emission [24].

In each time step, the solution is

$$\sigma(t + \delta t) = \exp(\mathcal{L}\delta t)\sigma(t), \tag{B5}$$

assuming $\mathcal{L}$ is constant throughout the time step δt. In this work, we consider only laser fields of constant amplitude, so that assumption holds. The matrix exponential applied to a vector V is found through its Taylor series in the form used in Horner's method, namely,

$$\exp(M)V \approx V + M\left(V + \frac{M}{2}\left(V + \frac{M}{3}\left(V + \frac{M}{4}V\right)\right)\right), \tag{B6}$$

here given to fourth order. We retain 30 terms, which puts a limit on the allowed time step given the energy splittings. Also we take $M = \mathcal{L}\delta t$ and $V = \sigma$. For a Hamiltonian including an electric field,

$$H(t) = H_0 + \mathcal{E}(t)d, \tag{B7}$$

where H_0 is the unperturbed atomic Hamiltonian, known for the subspace, and d is the dipole operator. If we were to treat all magnetic sublevels, this would be completely known for a vector electric field, e.g., as given in Refs. [19,20]. In this paper, the electric field is taken to be a scalar, and we use assumptions given at the end of Section 2 to avoid including the degenerate magnetic sublevels explicitly.

Funding. Air Force Research Laboratory (FA9451-23-P-0013); NIST Summer Undergraduate Research Fellowship.

Acknowledgment. Discussions with Paul Lett are gratefully acknowledged.

Disclosures. The authors declare no conflicts of interest.

Data availability. Specific functions that generated the curves are available from the authors upon reasonable request. Experimental points were digitized by the authors using figures in Refs. [12,14] using WebPlotDigitizer 4.6, available at [30].

REFERENCES

1. C. F. McCormick, V. Boyer, E. Arimondo, and P. D. Lett, "Strong relative intensity squeezing by four-wave mixing in rubidium vapor," Opt. Lett. **32**, 178–180 (2007).
2. J. Mika and L. Slodička, "High nonclassical correlations of large-bandwidth photon pairs generated in warm atomic vapor," J. Phys. B **53**, 145501 (2020).
3. M. Hosseini, B. M. Sparkes, G. Campbell, P. K. Lam, and B. C. Buchler, "High efficiency coherent optical memory with warm rubidium vapour," Nat. Commun. **2**, 174 (2011).
4. S. Wang, J. Yuan, L. Wang, L. Xiao, and S. Jia, "Characterization of rubidium thin cell properties with sandwiched structure using a multipath interferometer with an optical frequency comb," Opt. Lett. **46**, 4284–4287 (2021).
5. T. N. Bandi, "A comprehensive overview of atomic clocks and their applications," BEMS Rep. **9**, 1–10 (2023).
6. N. Ghahremani Arekhloo, H. Parvizi, S. Zuo, H. Wang, K. Nazarpour, J. Marquetand, and H. Heidari, "Alignment of magnetic sensing and clinical magnetomyography," Front. Neurosci. **17**, 1154572 (2023).
7. Y. Lu, T. Zhao, W. Zhu, L. Liu, X. Zhuang, G. Fang, and X. Zhang, "Recent progress of atomic magnetometers for geomagnetic applications," Sensors **23**, 5318 (2023).
8. R. Xu, A. Li, D. Li, and J. Yan, "Magneto-optical traps for cold atomic gravimetry: Research status and development trends," Appl. Sci. **13**, 6076 (2023).

9. S. Wang, J. Yuan, L. Wang, L. Xiao, and S. Jia, "All-optical information conversion in Rb vapor based on the spatial cross-phase modulation," Opt. Express **30**, 45517–45524 (2022).
10. R. Mottola, G. Buser, and P. Treutlein, "Quantum memory in a microfabricated rubidium vapor cell," arXiv, arXiv:2307.08538 (2023).
11. Q. Glorieux, T. Aladjidi, P. D. Lett, and R. Kaiser, "Hot atomic vapors for nonlinear and quantum optics," New J. Phys. **25**, 051201 (2023).
12. C. McCormick, D. Solli, R. Chiao, and J. Hickmann, "Saturable nonlinear refraction in hot atomic vapor," Phys. Rev. A **69**, 023804 (2004).
13. M. O. Araújo, H. L. de S. Cavalcante, M. Oriá, M. Chevrollier, T. P. de Silans, R. Castro, and D. Moretti, "Measurement of the Kerr nonlinear refractive index of Cs vapor," Phys. Rev. A **88**, 063818 (2013).
14. S. Wang, J. Yuan, L. Wang, L. Xiao, and S. Jia, "Measurement of the Kerr nonlinear refractive index of the Rb vapor based on an optical frequency comb using the z-scan method," Opt. Express **28**, 38334–38342 (2020).
15. F. D. Dos Santos, J. de Aquino Carvalho, G. Moura, and T. P. de Silans, "Measurement of the nonlinear refractive index of Cs D_1 line using z-scan," J. Opt. Soc. Am. B **36**, 2468–2472 (2019).
16. W. Gao, S. Wang, J. Yuan, L. Wang, L. Xiao, and S. Jia, "Sensitivity enhancement of nonlinear refractive index measurement by Gaussian-Bessel beam assisted z-scan method," Opt. Express **30**, 7291–7298 (2022).
17. C. McCormick, D. Solli, R. Chiao, and J. Hickmann, "Nonlinear absorption and refraction in near-detuned rubidium vapor," J. Opt. Soc. Am. B **20**, 2480–2483 (2003).
18. J. Wu, P. Jia, S. Wang, X. Wang, J. Yuan, L. Wang, Y. Hu, Z. Chen, and J. Xu, "Measuring saturable nonlinearity in atomic vapor via direct spatial mapping," Opt. Express **30**, 43012–43020 (2022).
19. D. A. Steck, "Rubidium 85 D line data," 2008, https://steck.us/alkalidata/rubidium85numbers.pdf.
20. D. A. Steck, "Rubidium 87 D line data," 2008, https://steck.us/alkalidata/rubidium87numbers.pdf.
21. R. H. Dicke, "Coherence in spontaneous radiation processes," Phys. Rev. **93**, 99–110 (1954).
22. D. Zeuch, F. Hassler, J. J. Slim, and D. P. DiVincenzo, "Exact rotating wave approximation," Ann. Phys. **423**, 168327 (2020).
23. M. Born and E. Wolf, *Principles of Optics: Electromagnetic Theory of Propagation, Interference and Diffraction of Light* (Elsevier, 2013).
24. G. Grynberg, A. Aspect, and C. Fabre, *Introduction to Quantum Optics: From the Semi-Classical Approach to Quantized Light* (Cambridge University, 2010).
25. P. J. Mohr and W. D. Phillips, "Dimensionless units in the SI," Metrologia **52**, 40–47 (2015).
26. A. Zangwill, *Modern Electrodynamics* (Cambridge University, 2013).
27. A. N. Sharma, Z. H. Levine, M. A. Ritter, K. H. Kagalwala, E. J. Weissler, E. A. Goldschmidt, and A. L. Migdall, "Photon echoes using atomic frequency combs in Pr:YSO-experiment and semiclassical theory," Opt. Express **31**, 4899–4919 (2023).
28. N. Korneev and C. G. Parra, "Vectorial mechanism of nonlinearity enhancement in rubidium vapor," J. Opt. Soc. Am. B **29**, 2588–2594 (2012).
29. C. Jirauschek, M. Riesch, and P. Tzenov, "Optoelectronic device simulations based on macroscopic Maxwell–Bloch equations," Adv. Theor. Simul. **2**, 1900018 (2019).
30. https://apps.automeris.io/wpd/.